I&EC research
Industrial & Engineering Chemistry Research

pubs.acs.org/IECR

Article

Highly Efficient Conversion of Lignin into Diethyl Maleate Catalyzed by Molybdenum-Based Hybrid Catalysts

Zhang-Min Li,* Cheng-Yong Guo, Guo-Wen Fang, Jian-Fei Li, Yan Zhou, Ming-Shuai Sun, and Duan-Jian Tao*

Cite This: *Ind. Eng. Chem. Res.* 2023, 62, 13780−13789

Read Online

ACCESS | Metrics & More | Article Recommendations | Supporting Information

ABSTRACT: The direct oxidative depolymerization of lignin, a natural aromatic heteropolymer, poses a significant challenge due to its intricate structure and interconnected cross-linked linkages. In this study, a cost-effective MoS_2−MoC@NC_{800} catalyst is developed and employed in the catalytic oxidative depolymerization of bamboo lignin by using ethanol as a solvent. Experimental results demonstrated that, at a moderate temperature of 150 °C over 3 h, 86.6% of bamboo lignin was transformed, producing 1374.2 mg g^{-1} of small-molecule esters, including 564.8 mg g^{-1} of diethyl maleate. The superior catalytic properties of the MoS_2−MoC@NC_{800} catalyst are attributed to the synergistic catalytic effects of α-MoC and MoS_2, which enabled the direct catalysis and ring opening of the aromatic rings in lignin and subsequent esterification with ethanol to generate small-molecule ester products. The detailed characterizations and control experiments reinforced these findings. This study offers promising opportunities for the utilization of green and sustainable lignin resources in the production of high-value small-molecule chemicals.

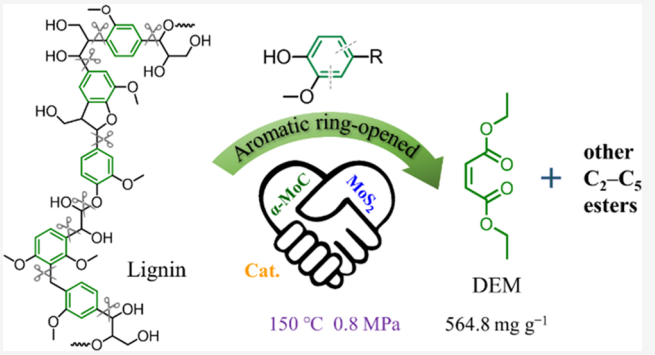

INTRODUCTION

The conversion of biomass into chemicals has become a priority for reducing dependence on fossil fuels and mitigating greenhouse gas emissions.[1−3] Biomass is a renewable source of carbohydrates that immobilizes CO_2, producing approximately 170 billion tons per year.[1,4−6] Lignin, a natural aromatic heteropolymer, accounts for ∼40% of the energy content and 10−35% of the weight of lignocellulosic materials.[7] Lignin is composed of sinapyl alcohol, coniferyl alcohol, and *p*-coumaric alcohol, which are connected by β-O-4, β-5, 5-5, and other linkages.[8,9] Despite the abundance of lignin, only ∼3% is currently utilized for commercial applications,[10] and the rest is typically burned, resulting in air pollution.[11] Consequently, an efficient valorization strategy is required for the effective utilization of lignin. Various methods are available for converting lignin into valuable fuels and chemicals,[12] including oxidative depolymerization, which offers several advantages. This approach focuses on the production of high-value oxygenated platform aromatic or aliphatic small-molecule compounds, which can be employed as raw materials in the chemical and pharmaceutical industries.

Significant efforts have been devoted to the use of homogeneous catalysts for the oxidative depolymerization of lignin.[13,14] However, isolation of the resulting products is complex and expensive, which limits their industrial applicability. While noble metals like Au, Pd, and Ru are highly efficient and selective for lignin valorization, their use is not practical due to their high cost, toxicity, and reliance on external H_2.[15] Therefore, there is a pressing need for the transformation of lignin using low-cost heterogeneous catalysts. Nitrogen-doped carbon-loaded metal materials have garnered significant interest due to their high concentration of oxygen-containing groups, excellent dispersibility, easy modification reactivity, and favorable properties.[16−22] Moreover, the addition of N dopants can improve the catalytic activity of nitrogen-doped carbon-supported metal catalysts by enhancing the conductivity between metal sites and carbon substrates.[23]

Ma et al.[24] were able to fully depolymerize Kraft lignin using MoC_{1-x}/activated carbon, resulting in the production of monophenol esters and benzyl alcohols. Wu et al.[25] also achieved depolymerization of lignin to aromatic products at 280 °C using α- and β-MoC_{1-x}. While these studies demonstrate impressive catalytic effects, most MoC catalysts require high temperatures and mainly facilitate the breaking of the C−O bond in lignin, resulting in the production of

Received: June 1, 2023
Revised: August 9, 2023
Accepted: August 10, 2023
Published: August 28, 2023

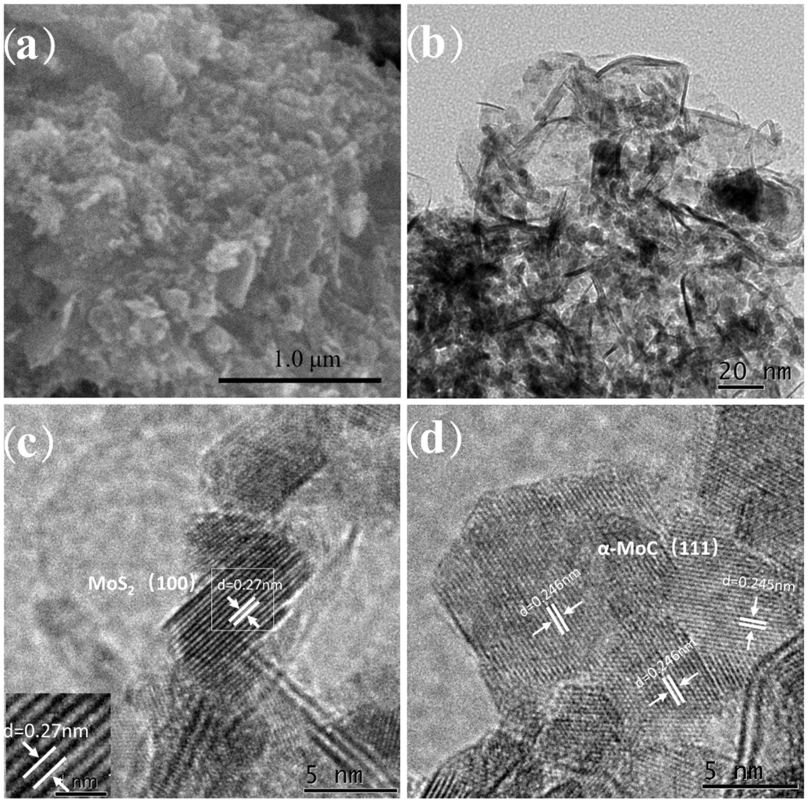

Figure 1. (a) SEM, (b) TEM, and (c, d) HR-TEM images of the MoS_2−MoC@NC_{800} catalyst.

aromatic monomers.[26−31] A more practical approach is to achieve the efficient catalytic depolymerization of lignin directly to obtain ring-opening small-molecule products in a single step. Chemical thermal catalysis has been used to obtain small-molecule volatiles in some studies,[32−36] but the resulting product composition is often complex and difficult to separate due to the nonspecific bond-breaking process of the Fenton reaction. Recently, Li and his team developed a series of metal-containing catalysts that selectively depolymerize lignin and produce small-molecule products with diethyl maleate (DEM) as the main product.[37,38] DEM is widely used as a platform chemical in polymers, fragrances, and pesticides, which are typically derived from the petrochemical industry.[37,39] This work lays the foundation for the selective production of small-molecule chemicals from lignin. However, there is still a need for further research to improve the yields of DEM and other volatile chemicals.

Previous research has conclusively shown that MoS_2 boasts exceptional catalytic activity in the conversion of lignin.[40] Building upon these findings, this study successfully employed molybdenum-based hybrid catalysts, which incorporate MoC and MoS_2, to achieve the depolymerization of lignin. This was achieved by cleaving the interconnecting bonds and selectively opening the aromatic rings, resulting in remarkable yields of DEM and other volatile chemicals. Moreover, this study diligently optimized critical reaction parameters, such as temperature, time, and O_2 pressure. The catalyst underwent comprehensive characterization, and the researchers thoroughly explored the reaction process. To gain a deep understanding of the catalytic process and mechanism, both pre- and postreaction assessments of the lignin were conducted, thereby acquiring valuable insights.

EXPERIMENTAL SECTION

Synthesis of the MoS_2−MoC@NC Catalyst. In this procedure, Pluronic P123 (1.0 g), melamine (7.0 g), and $(NH_4)_6Mo_7O_{24}{\cdot}4H_2O$ (0.5 g) were dissolved in 100 mL of distilled water and reacted in a flask at 100 °C for 1 h. Next, 5.0 g of 20% sulfuric acid was added to the flask dropwise, and the reaction continued for 20 min. After the mixture cooled, a solid−liquid mixture was obtained, and the precipitate was strained out and washed three times with distilled water. The precipitate was dried at 60 °C, ground to powder, and placed into a tube furnace under an N_2 atmosphere. The powder was then heated to 800 °C at 5 °C/min for 2 h, resulting in the formation of a black solid powder, denoted as MoS_2−MoC@NC_{800}. MoC@NC_{700} was also synthesized in a manner similar to MoS_2−MoC@NC_{800}, but with a calcining temperature of 700 °C. For comparison, a MoC@NC_{800} catalyst was synthesized similarly to MoS_2−MoC@NC_{800}, but without the addition of sulfuric acid.

Catalytic Performance Analysis. 25 mg of bamboo lignin, 70 mg of catalyst, and 7.0 mL of ethanol were transferred into a 50.0 mL autoclave. Oxygen was then used to purge the autoclave for 5 cycles. The reaction was conducted by stirring the mixture at 650 rpm at the required temperature and O_2 pressure, and at the end of the reaction, the reactor was cooled down. The resulting mixture was separated through centrifugation, and the filtrate was washed with ethanol three times. The washed ethanol solution was mixed with the filtrate and an internal standard (dimethyl phthalate) before being subjected to analysis via gas chromatography−mass spectrometry (GC-MS) and GC-flame ionization detector (FID). The remaining solution was transferred to a beaker containing 150 mL of distilled water, left to precipitate, and then filtered through an organic filter membrane with a pore size below 0.2

https://doi.org/10.1021/acs.iecr.3c01826
Ind. Eng. Chem. Res. 2023, 62, 13780−13789

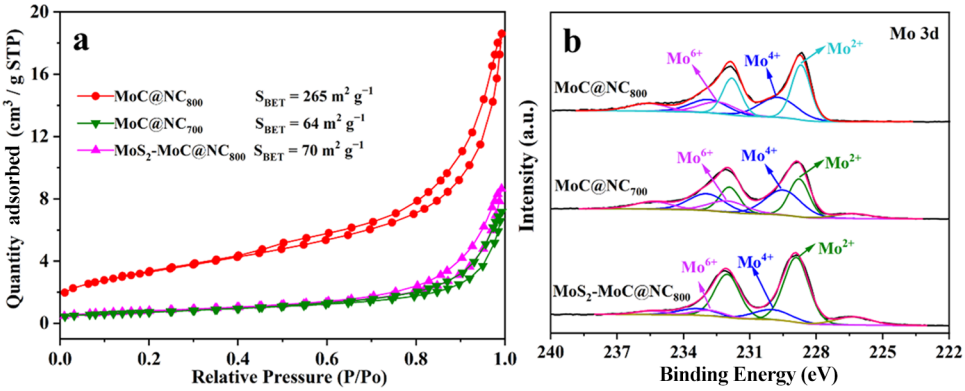

Figure 2. (a) N_2 adsorption−desorption isotherms and (b) XPS spectra of Mo 3d of MoS_2−MoC@NC_{800}, MoC@NC_{700}, and MoC@NC_{800} catalysts.

μm. The filter residue was washed and dried at 60 °C to obtain lignin char.

Lignin conversion (Conv.) and the yield of DEM (Y_{DEM}) and other products (Y_{others}) were obtained using eqs 1 to 3. W_F and W_C represent the weights of feedstock and reaction residue, respectively. W_{DEM} and W_{others} represent the yields of DEM and other products obtained by GC-FID, respectively.

$$\text{Conv. (\%)} = \frac{W_F - W_C}{W_F} \times 100\% \quad (1)$$

$$Y_{DEM}\ (\text{mg g}^{-1}) = \frac{W_{DEM}}{W_F} \times 1000 \quad (2)$$

$$Y_{others}\ (\text{mg g}^{-1}) = \frac{W_{others}}{W_F} \times 1000 \quad (3)$$

RESULTS AND DISCUSSION

Catalyst Characterization. The synthesized catalysts, including MoC@NC_{800}, MoC@NC_{700}, and MoS_2−MoC@NC_{800}, were subjected to X-ray diffraction (XRD) analysis, and the resulting XRD spectra are presented in Figure S1. The XRD analysis reveals that the peaks observed at 2θ = 37.1, 43.1, and 62.7° correspond to the (111), (200), and (220) crystallographic planes, respectively, of the α-MoC crystalline phase (PDF#03−0907).[41] Moreover, the characteristic peaks of the α-MoC crystalline phase became narrower with an increasing calcination temperature, suggesting an improvement in the crystallinity of the catalyst. A comparison of MoC@NC_{800} with MoC@NC_{700} and MoS_2−MoC@NC_{800} reveals that the crystalline phase of α-MoC is retained in the latter two catalysts. This suggests that sulfuric acid does not impair the α-MoC phase during the synthesis of the catalysts. Interestingly, the addition of sulfuric acid during calcination resulted in the formation of a new MoS_2 crystalline phase, as evidenced by the peaks at 2θ = 14.2, 32.9, and 59.2°, which correspond to the (002), (100), and (110) crystalline planes of MoS_2 (PDF#75-1539), respectively. Moreover, the MoS_2 crystalline phases are significantly influenced by temperature, with a high temperature promoting the generation of the MoS_2 crystal phase. As illustrated in Figure S1, no obvious MoS_2 crystalline phase was detected in the MoC@NC_{700} catalyst. However, when the calcination temperature is increased to 800 °C, the MoS_2 crystalline phase is observed in the MoS_2−MoC@NC_{800} catalyst. This indicates that an elevated calcination temperature of 800 °C facilitates the formation of both α-MoC and MoS_2 phases in the MoS_2−MoC@NC_{800} catalyst.

The morphology and structure of the MoS_2−MoC@NC_{800} catalyst were characterized by scanning electron microscopy (SEM) and transmission electron microscopy (TEM), as shown in Figure 1. The SEM image presented in Figure 1a reveals that the MoS_2−MoC@NC_{800} catalyst exhibits a loosely packed surface with a uniform distribution and an absence of visible agglomerates. The TEM image in Figure 1b illustrates that the metal particles are distributed uniformly on the support material of the MoS_2−MoC@NC_{800} catalyst. The high-resolution (HR)-TEM images presented in Figure 1c,d confirms that the measured crystal plane spacings of 0.27 and 0.246 nm correspond to the (110) lattice of MoS_2 and the (111) lattice of α-MoC, respectively.[42] Moreover, a uniform distribution of MoS_2 particles on the support material is observed, and elemental mapping further confirms that the Mo, S, C, N, and O elements are uniformly distributed throughout the MoS_2−MoC@NC_{800} catalyst (Figure S2), consistent with the XRD results in Figure S1. Additionally, the SEM image of MoC@NC_{700} (Figure S3) shows that MoC@NC_{700} exhibits a morphology similar to that of MoS_2−MoC@NC_{800}.

Figure 2a depicts the N_2 adsorption−desorption isotherms of the MoC@NC_{800}, MoC@NC_{700}, and MoS_2−MoC@NC_{800} catalysts. The results indicate that these samples had a type II isotherm with an H3 hysteresis loop, suggesting that they are mesoporous materials. The specific surface area of MoC@NC_{800} is found to be 265 $m^2\ g^{-1}$. Meanwhile, the specific surface areas of MoC@NC_{700} and MoS_2−MoC@NC_{800} decrease to 64 and 78 $m^2\ g^{-1}$, respectively. To further explore the surface elemental composition of MoC@NC_{800}, MoC@NC_{700}, and MoS_2−MoC@NC_{800} catalysts, X-ray photoelectron spectroscopy (XPS) spectral characterization was carried out, as shown in Figure S4 and Table S1. The full-scan spectra of the MoS_2−MoC@NC_{800} catalyst reveal the presence of C, N, O, S, and Mo elements. The XPS fine spectra of Mo 3d are displayed in Figure 2b, three peaks are corresponding to Mo^{2+}, Mo^{4+}, and Mo^{6+}, respectively.[43−45] Compared with MoC@NC_{700} and MoC@NC_{800}, MoS_2−MoC@NC_{800} has more Mo^{2+}, confirming the presence of many MoS_2 crystalline phases in MoS_2−MoC@NC_{800}. The contents of the valence states of the Mo elements listed in Table S2 further show that MoS_2−MoC@NC_{800} contains up to 74.7% Mo^{2+}, only 17.4% Mo^{4+}, and 7.9% Mo^{6+}, whereas MoC@NC_{700} contains only 36.7% Mo^{2+}, up to 43% Mo^{4+}, and 20.3% Mo^{6+}. The prevailing

https://doi.org/10.1021/acs.iecr.3c01826
Ind. Eng. Chem. Res. 2023, 62, 13780−13789

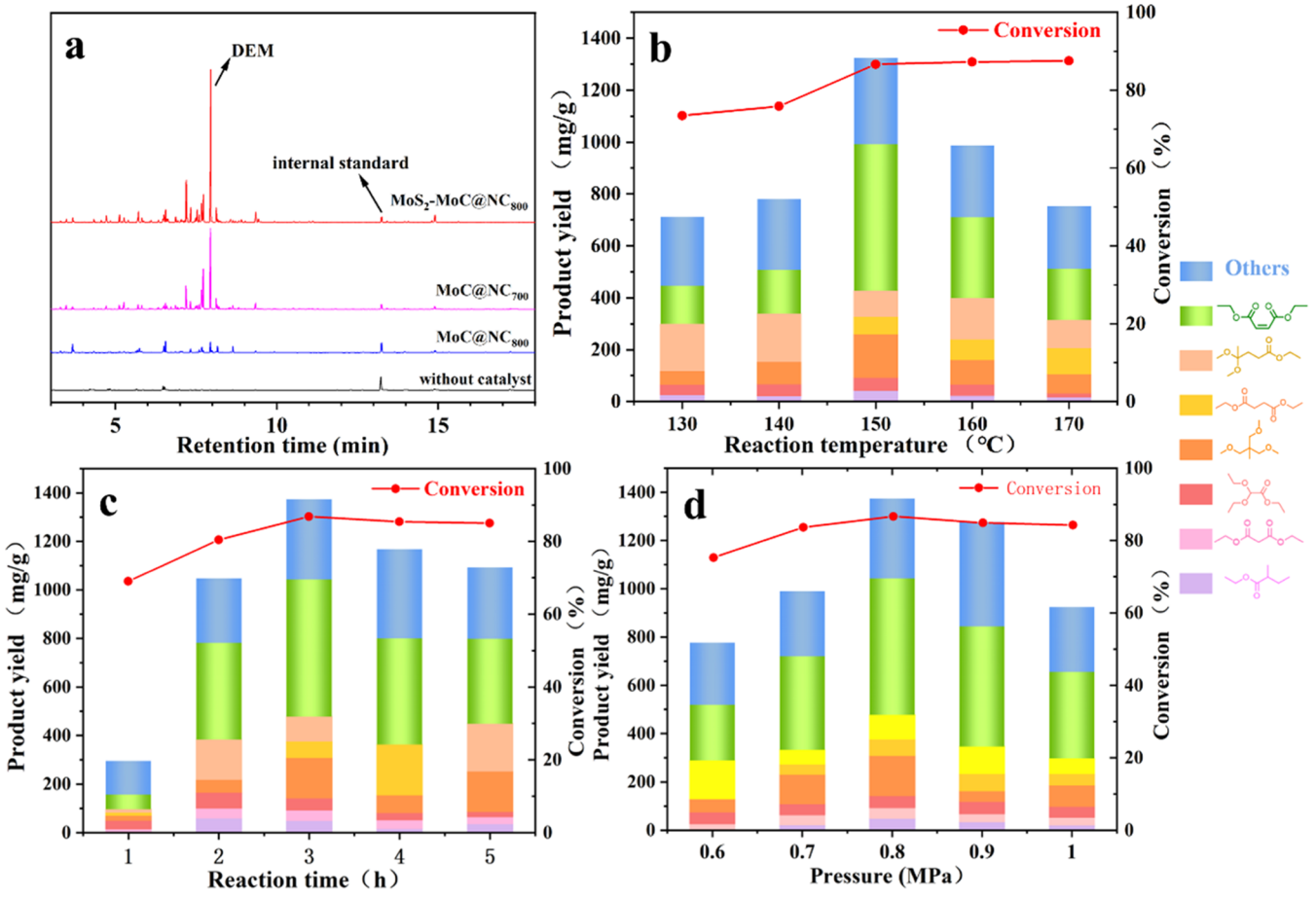

Figure 3. (a) GC-FID spectra of the volatile products derived from the lignin over different catalysts and influence of (b) reaction temperature, (c) reaction time, and (d) the pressure of O_2 on product distribution.

Table 1. Selective Catalytic Oxidation of Lignin[a]

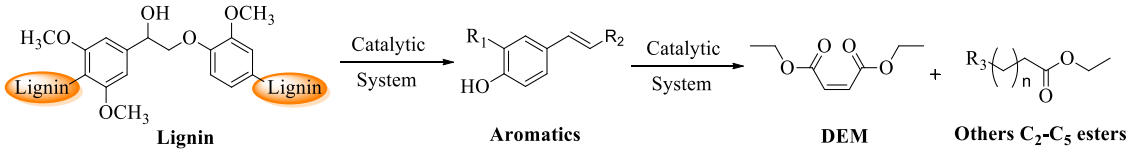

entry	catalyst	conv. (%)	yield (mg g^{-1}) DEM	Others C_2–C_5 esters	aromatics	ref
1	none	51.8	0.0	39.3	8.9	this work
2	MoS_2	59.9	7.9	75.2	12.6	this work
3	$MoC@NC_{800}$	63.7	32.0	216.1	15.2	this work
4	$MoC@NC_{700}$	80.5	348.1	611.6	14.0	this work
5	MoS_2–$MoC@NC_{800}$	86.6	564.8	715.9	29.4	this work
6[b]	$[BMIM]Fe_2Cl_7$-$[BSMIM]HSO_4$	73.5	158.5	78.3	31.0	ref 46
7[c]	15Ce-5Cu/MFI-ns	81.6	180.9	62.3	50.8	ref 37
8[d]	$[BSmim]CuPW_{12}O_{40}$	92.9	404.8			ref 38

[a]Reaction conditions: lignin (25 mg), catalyst (70 mg), EtOH (7.0 mL), O_2 (0.8 MPa), 150 °C, 3 h. [b]Conditions: lignin (25 mg), catalyst (1.0 mmol), EtOH (20.0 mL), O_2 (1.0 MPa), 160 °C, 5 h. [c]Conditions: lignin (100 mg), catalyst (100 mg), ethanol (5.0 mL), oxygen (1.0 MPa), 150 °C, 24 h. [d]Conditions: lignin (250 mg), catalyst (0.9 mmol), EtOH/H_2O (20 mL), O_2 (0.8 MPa), 160 °C, 5 h.

view in the scientific community is that low-valent Mo ions exhibit superior catalytic activity in oxidation processes. In addition, α-MoC crystalline phases also exist in MoS_2–MoC@NC_{800} catalyst (Figure 1).

Depolymerization Performance Analysis. The catalytic performance of the Mo-based catalysts in the depolymerization of lignin was assessed by detecting the volatile products by using GC-MS, as shown in Figure 3a. When the MoS_2–MoC@NC_{800} catalyst is utilized, a significant increase in catalytic activity is observed with a DEM yield of 564.8 mg per gram of lignin at 7.95 min. The details of all detected volatile products, including their peak time, name, structural formula, molecular formula, and molecular weight, are collated and presented in Table S3.

https://doi.org/10.1021/acs.iecr.3c01826
Ind. Eng. Chem. Res. 2023, 62, 13780−13789

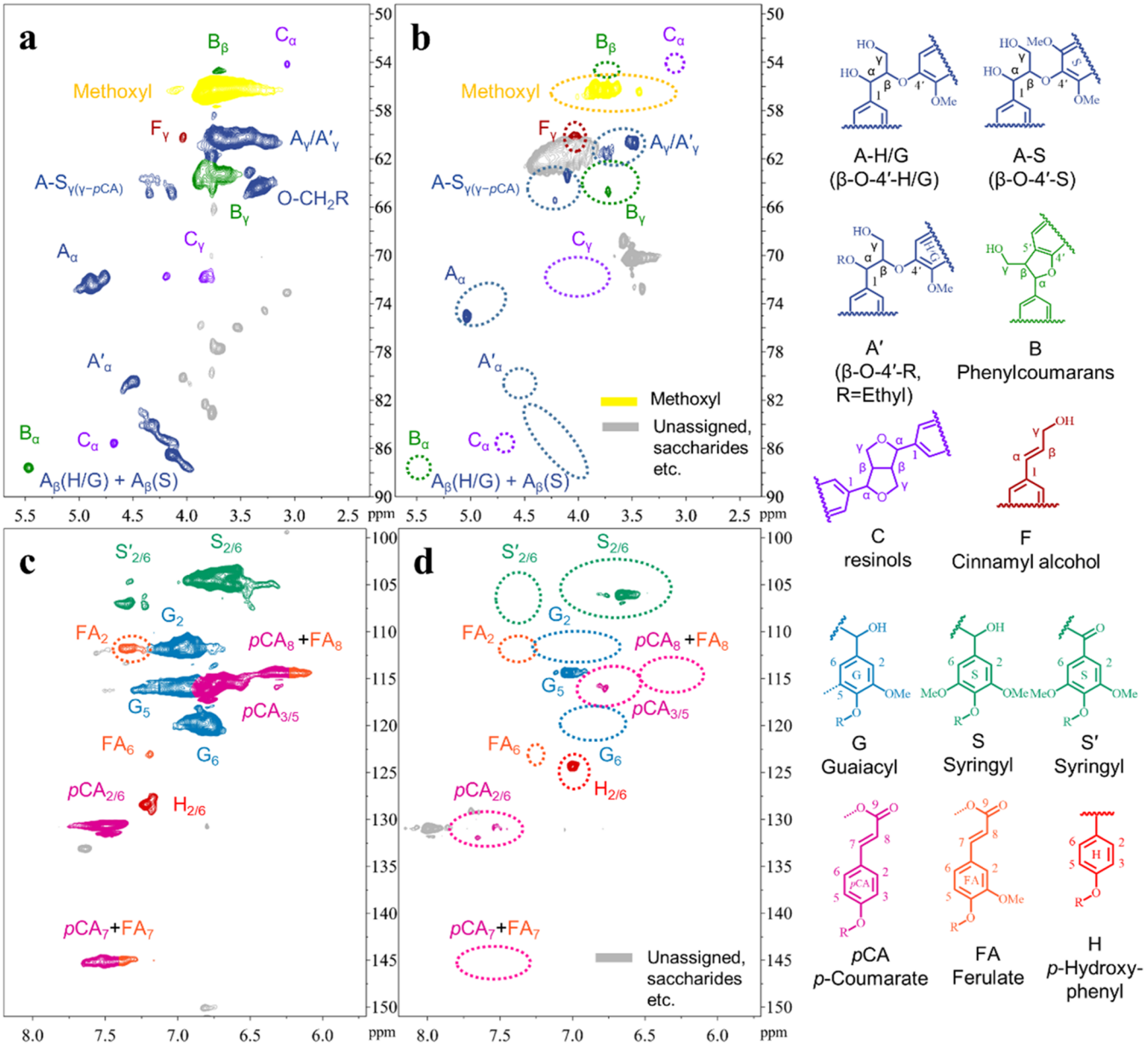

Figure 4. 2D HSQC NMR spectra of original lignin (a, c) and lignin char (b, d).

Table 1 presents the catalytic performance of different catalysts used for depolymerizing lignin, along with a comparison with literature values.[37,38] It is found that the absence of a catalyst or the use of bulk MoS_2 leads to unsatisfactory yields of volatile products, with a negligible DEM yield obtained (Table 1, entries 1 and 2). $MoC@NC_{800}$ catalyst has only α-MoC active site without MoS_2 active site and also has little DEM yield, but the lignin conversion has increased significantly (Table 1, entry 3). This suggests that $MoC@NC_{800}$ holding α-MoC active sites can effectively catalyze the breakage of the C−O (β-O-4) bonds in lignin, thereby increasing the lignin conversion. When the MoS_2−$MoC@NC_{800}$ catalyst containing both α-MoC and MoS_2 active sites is utilized, as shown in Figure 3a, the best experimental performance is observed, producing 564.8 mg g^{-1} DEM on an 86.6% lignin conversion (Table 1, entry 5). Thus, MoS_2 and α-MoC are presumably active sites for the efficient depolymerization of lignin.

Meanwhile, the performances of other catalysts for depolymerization of lignin to DEM are listed in Table 1.[37,38,46] For example, Li and co-workers reported the polyoxometalate ionic liquid $[BSmim]CuPW_{12}O_{40}$ catalyst for oxidating lignin in air under 160 °C for 5 h, producing the yield of DEM with 404.8 mg g^{-1}.[38] Later, they further synthesized hierarchical Ce−Cu/MFI nanosheets for lignin oxidation under 150 °C for 24 h, yielding 180.9 mg g^{-1} DEM with 61.5% selectivity.[37] Recently, Zhao et al. used the cooperative acidic ionic liquid pair of $[BMIM]Fe_2Cl_7$-$[BSMIM]HSO_4$ for cleaving the lignin aromatic ring to obtain DEM under 160 °C for 5 h, with a yield of 158.5 mg g^{-1} and 44.25% selectivity.[46] Compared with the above-mentioned results, the MoS_2−$MoC@NC_{800}$ catalyst shows the highest yield of DEM (Table 1, entries 5−8). Both MoS_2 and α-MoC active sites in the MoS_2−$MoC@NC_{800}$ catalyst can promote the cleavage of both C−O and C−C bonds in lignin, which contributes to such superior catalytic performance. These

https://doi.org/10.1021/acs.iecr.3c01826
Ind. Eng. Chem. Res. 2023, 62, 13780−13789

Scheme 1. Differences in the Oxidative Properties of Lignin Model Compounds

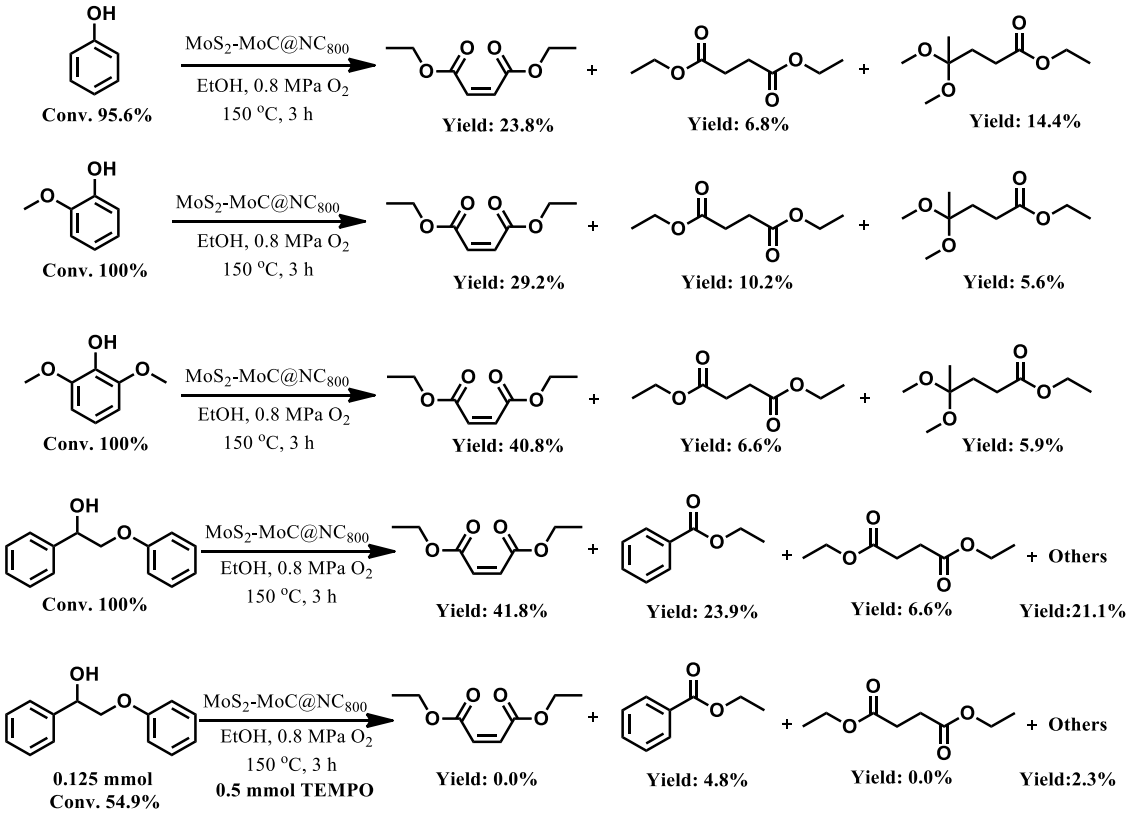

results highlight the essential role of metallic molybdenum in improving the lignin conversion and DEM yield, particularly the MoS_2 and α-MoC species in MoS_2−MoC@NC_{800} that significantly enhance the catalytic performance of the catalyst.

The product distribution and selectivity in a reaction are often found to be directly dependent on the reaction temperature. To investigate the impact of the experimental temperature, the conversion of lignin and the yield of the primary products are analyzed. As shown in Figure 3b, an increase in both lignin conversion and total volatile product yield is observed as the temperature is raised from 130 to 150 °C. Specifically, the lignin conversion increases from 73.4 to 86.6%, while the total ester yield increases from 727.3 to 1374.2 mg g^{-1}, with the yield of DEM peaking at 564.8 mg g^{-1}. Nevertheless, an observed decline in the overall yield of ester products occurs when the temperature is increased beyond 150 to 170 °C. This decrease can be attributed to the accelerated oxidation and decomposition of ester products into smaller molecules, which is more pronounced at higher temperatures. This outcome aligns with the majority of previous findings documented in the literature.[47,48]

The influence of the reaction time on lignin depolymerization to produce DEM is also systematically investigated, considering its significance for industrial production and energy conservation. As presented in Figure 3c, the lignin conversion and DEM yield exhibit an improvement upon extending the reaction time from 1 to 3 h, particularly between 1 and 2 h, whereby the DEM yield is enhanced by over 350 mg g^{-1}. This is attributed to the generation of more lignin fragments that undergo catalytic ring opening to generate DEM. The maximum DEM yield is obtained at 3 h of reaction. However, when the reaction time is extended to 5 h, the lignin conversion rate remains unchanged while the DEM yield decreases. This is because the prolonged reaction time would lead to further oxidative decomposition of DEM to form smaller molecules. Based on the above results, a reaction time of 3 h is identified as the optimal reaction time for this catalytic reaction.

The impact of primary O_2 pressure on lignin concentration and volatile product yield is studied with the MoS_2−MoC@NC_{800} catalyst. As depicted in Figure 3d, an increase in initial O_2 pressure (0.6−0.8 MPa) results in a corresponding increase in both lignin conversion and yield of volatile chemicals, such as DEM. The maximum lignin conversion (86.6%) and DEM yield (564.8 mg g^{-1}) is achieved at an O_2 pressure of 0.8 MPa. However, further enhancement of the initial O_2 pressure from 0.8 to 1.0 MPa results in a decrease in lignin conversion rate and DEM yield. This indicates that an O_2 pressure above 0.8 MPa leads to excessive oxidation and decomposition. Therefore, the optimized initial pressure of the O_2 is 0.8 MPa. Based on the optimized parameters mentioned above, the optimal reaction conditions for this work are 150 °C, 3 h reaction time, and 0.8 MPa initial O_2 pressure.

Lignin Characterization. To investigate the structural changes of lignin during catalytic oxidation, the lignin was characterized pre- and post-experiment. The Fourier transform infrared (FT-IR) spectra of the raw lignin and the lignin char are presented in Figure S5. The difference in FT-IR absorption peaks between the raw lignin and lignin char indicates effective depolymerization of lignin. In comparison to raw lignin, the lignin char exhibits the appearance of three distinctive vibrational peaks at 1604, 1513, and 1459 cm^{-1}, which can be attributed to the characteristic peaks of the benzene ring that had either disappeared or weakened significantly. This observation suggests that the aromatic ring in lignin underwent conversion. Moreover, the presence of a vibrational peak at

https://doi.org/10.1021/acs.iecr.3c01826
Ind. Eng. Chem. Res. 2023, 62, 13780−13789

1728 cm^{-1}, which belongs to nonconjugated carbonyl vibration, indicated the generation of numerous carbonyl groups during lignin depolymerization, consistent with the experimental findings presented in Table 1.

To gain a deeper understanding of the process of lignin depolymerization and the changes in its structure, two-dimensional (2D) heteronuclear single quantum coherence (HSQC) NMR characterization was conducted on the collected lignin before and after the reaction (Figure 4), with detailed peak allocations referenced from the literature.[47−52] First, the aliphatic regions (δ_C/δ_H 49−90/2.3−5.7) of the raw lignin and lignin char are compared. It is observed that the original lignin exhibited the characteristics of organosolv lignin, with a high number of β-O-4 bonds (blue region), methoxy (yellow region), a small amount of α-O-4 structure (green region), and few other C−O or C−C bonds. Conversely, after catalytic depolymerization using the MoS_2−MoC@NC_{800} catalyst, the content of β-O-4 and α-O-4 bonds, as well as methoxy, in the resulting lignin char is notably reduced (Figure 4a,b). These findings suggest that a significant proportion of C−O linkage bonds present in the lignin were cleaved during this catalytic depolymerization process.

The 2D HSQC NMR analysis conducted on the aromatic region (δ_C/δ_H 99−151/5.7−8.2) of the lignin (Figure 4c,d) demonstrates that the bamboo lignin shares the H, G, and S structural features characteristic of bamboo lignin. However, a comparison of the pre- and postreaction samples demonstrates that the S structural unit as well as most of the G and H units are no longer present, consistent with the aforementioned results for the aliphatic region, indicating that the G, S, and H units underwent catalytic conversion. Additionally, the majority of the pCA and FA structural units in the lignin disappear (Figure 4c,d in purple), indicating that the majority of the aromatic structural units are cleaved, and only smaller benzene rings remain in the lignin char, such as G_5, $H_{2/6}$, and a small amount of $pCA_{3/5}$ unit. This outcome reconfirms that units containing methoxy on the benzene ring are more susceptible to catalytic transformation in the reaction. It is the catalytic conversion of all three lignin units (H, G, and S) that explains the higher DEM yield (564.8 mg g^{-1}) in this study than that reported in the literature.[37,38]

Table S4 illustrates the changes in the elemental composition of lignin throughout the catalytic conversion process. The lignin char exhibits a notable reduction in elemental C and H content, while the O content is increased, revealing a significant transformation in the chemical structure of lignin. These changes suggest that a greater proportion of C and H elements in lignin have been converted to volatile products. The data indicates that approximately 54.2% of carbon has been converted into raw lignin, with 15.8% being transformed into the primary product DEM, based on calculations.

Catalytic Mechanism Analysis. To study the possible mechanism underlying lignin depolymerization, the MoS_2−MoC@NC_{800} catalyst was employed to react with several lignin model compounds, including phenol, guaiacol, 2,6-dimethoxyphenol, and 2-phenoxy-1-phenylethanol. These model compounds contain the H, G, and S structural units as well as the β-O-4 bonds of lignin. Scheme 1 demonstrates that all of the model compounds undergo oxidative ring opening to produce small-molecule ester products, with DEM being the primary product. This observation suggests that the C−O ether bond is indeed cleaved and that the aromatic units are converted to DEM through ring opening during the reaction process. These results are in good agreement with the results from 2D HSQC NMR characterization. To verify whether the reaction is a radical process, a radical quenching agent (TEMPO) was introduced in 4-fold excess to the model compound. The last reaction equation in Scheme 1 indicates that the transformation of the lignin model compound and the yield of DEM are considerably diminished in the presence of TEMPO. This suggests that the lignin ring-opening process is a free radical reaction process.

To investigate the free radicals involved in the lignin depolymerization process, electron paramagnetic resonance (EPR) experiments were conducted, and the results are illustrated in Figure 5. It is observed that no signal is detected

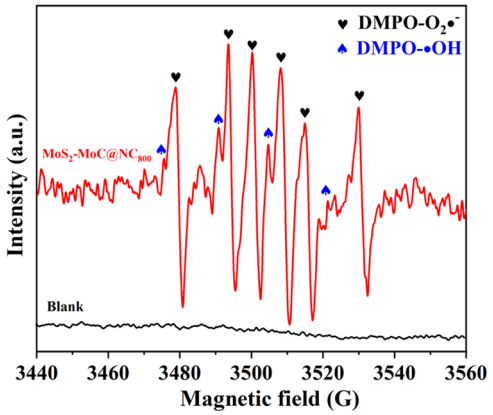

Figure 5. EPR spectra of DMPO-$O_2^{\bullet-}$ and DMPO-$^{\bullet}$OH adducts of different samples in the presence of DMPO.

in the absence of the catalyst. Upon loading the MoS_2−MoC@NC_{800} catalyst, hydroxyl and peroxyl radical signals are detected within 1.5 h of the reaction. This indicates that the oxidative ring opening of lignin involves both peroxyl and hydroxyl radicals. Based on the above findings, a plausible lignin depolymerization mechanism is proposed. Initially, the C−O bond in lignin is oxidized and cleaved to form a monophenolic intermediate. Then, under the influence of hydroxyl and peroxyl radicals, the aromatic rings are oxidized and ring-opened to produce the maleic aldehyde intermediate. This is further oxidized to maleic acid via aqueous O_2 and esterified with ethanol solvent, resulting in the final product of DEM. The proposed reaction pathway is presented in Scheme 2.

After the reaction, the MoS_2−MoC@NC_{800} catalyst was retrieved, dried, calcined, and reused in a subsequent experiment. However, it is observed that the yield of products and the lignin conversion rate are lower compared to when a fresh catalyst was used (Table S5). To determine the reasons for the decrease in catalyst activity, the catalyst was characterized by XRD analysis before and after recovery (Figure S6). The results indicate that the crystallinity of MoS_2 in the recovered catalyst is significantly reduced compared with the original catalyst. However, the MoO_3 crystalline phase was detected obviously in the recycle MoS_2−MoC@NC_{800} catalyst. This change contributes to the poor cycle performance of the MoS_2−MoC@NC_{800} catalyst, which is consistent with previous reports in the literature.[41]

https://doi.org/10.1021/acs.iecr.3c01826
Ind. Eng. Chem. Res. 2023, 62, 13780−13789

Scheme 2. Proposed Reaction Pathway for the Selective Breakage of Lignin to Produce DEM

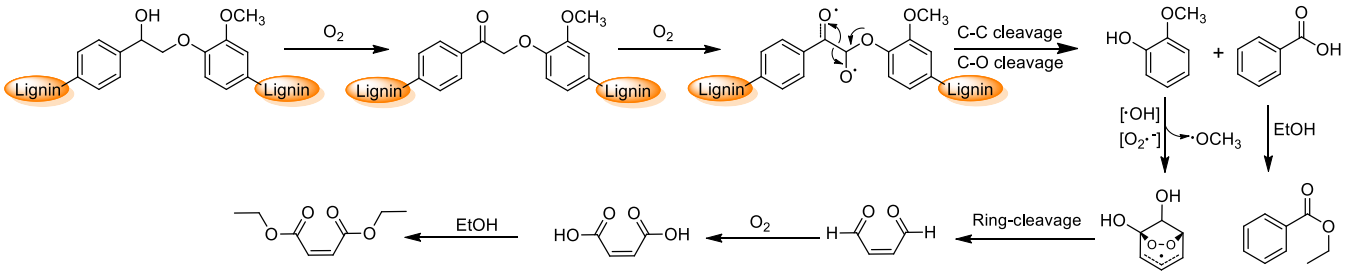

CONCLUSIONS

In summary, a highly efficient and cost-effective MoS_2−MoC@NC_{800} catalyst containing two active centers (α-MoC and MoS_2) was developed for the depolymerization of bamboo lignin. The catalyst is capable of catalyzing lignin to form valuable low-molecular-weight compounds at a mild reaction condition (150 °C for 3 h), with 86.6% of the lignin being transformed and yielding 1374.2 mg g^{-1} volatile compounds, including 564.8 mg g^{-1} of DEM. The characterization of the catalyst reveals that the highly dispersed α-MoC and MoS_2 nanoparticles functioned as catalytically active centers and exhibited a strong synergistic effect in promoting the efficient oxidative depolymerization of lignin. Based on the results of mechanistic studies, it is suggested that the depolymerization of lignin occurs initially through the cleavage of C−O and C−C bonds, leading to the formation of monophenols. Subsequently, these aromatic intermediates undergo ring opening, accompanied by simultaneous esterification reactions. This intricate process ultimately yields the selective production of DEM and other C_2−C_5 ester compounds. Hence, this study presents a novel approach for designing solid catalysts with MoS_2 and MoC active sites, enabling efficient radical reactions. This breakthrough offers promising prospects for the future transformation of lignin into high-value-added products.

ASSOCIATED CONTENT

Supporting Information

The Supporting Information is available free of charge at https://pubs.acs.org/doi/10.1021/acs.iecr.3c01826.

Materials, procedures, additional experiments, analysis, and characterization data (XRD, EDS elemental mapping, XPS, GC-MS products, FT-IR, and SEM) (PDF)

AUTHOR INFORMATION

Corresponding Authors

Zhang-Min Li − *National Engineering Research Center for Carbohydrate Synthesis, Key Laboratory of Fluorine and Silicon for Energy Materials and Chemistry of Ministry of Education, College of Chemistry and Chemical Engineering, Jiangxi Normal University, Nanchang 330022, China*; Email: zmli@jxnu.edu.cn

Duan-Jian Tao − *National Engineering Research Center for Carbohydrate Synthesis, Key Laboratory of Fluorine and Silicon for Energy Materials and Chemistry of Ministry of Education, College of Chemistry and Chemical Engineering, Jiangxi Normal University, Nanchang 330022, China*; orcid.org/0000-0002-8835-0341; Email: djtao@jxnu.edu.cn

Authors

Cheng-Yong Guo − *National Engineering Research Center for Carbohydrate Synthesis, Key Laboratory of Fluorine and Silicon for Energy Materials and Chemistry of Ministry of Education, College of Chemistry and Chemical Engineering, Jiangxi Normal University, Nanchang 330022, China*

Guo-Wen Fang − *National Engineering Research Center for Carbohydrate Synthesis, Key Laboratory of Fluorine and Silicon for Energy Materials and Chemistry of Ministry of Education, College of Chemistry and Chemical Engineering, Jiangxi Normal University, Nanchang 330022, China*

Jian-Fei Li − *National Engineering Research Center for Carbohydrate Synthesis, Key Laboratory of Fluorine and Silicon for Energy Materials and Chemistry of Ministry of Education, College of Chemistry and Chemical Engineering, Jiangxi Normal University, Nanchang 330022, China*

Yan Zhou − *National Engineering Research Center for Carbohydrate Synthesis, Key Laboratory of Fluorine and Silicon for Energy Materials and Chemistry of Ministry of Education, College of Chemistry and Chemical Engineering, Jiangxi Normal University, Nanchang 330022, China*; orcid.org/0000-0003-0108-5061

Ming-Shuai Sun − *National Engineering Research Center for Carbohydrate Synthesis, Key Laboratory of Fluorine and Silicon for Energy Materials and Chemistry of Ministry of Education, College of Chemistry and Chemical Engineering, Jiangxi Normal University, Nanchang 330022, China*; orcid.org/0000-0002-5126-4159

Complete contact information is available at: https://pubs.acs.org/10.1021/acs.iecr.3c01826

Notes

The authors declare no competing financial interest.

ACKNOWLEDGMENTS

This work was financially supported by the National Natural Science Foundations of China (22068013), the Natural Science Foundations of Jiangxi Province (20232BAB203052), the Key Research and Development Program of Jiangxi Province (20202BBGL73118), as well as the Key Lab of Fluorine and Silicon for Energy Materials and Chemistry of Ministry of Education, Jiangxi Normal University (KFSEMC-202209).

REFERENCES

(1) Schutyser, W.; Renders, T.; Van den Bosch, S.; Koelewijn, S. F.; Beckham, G. T.; Sels, B. F. Chemicals from Lignin: An Interplay of Lignocellulose Fractionation, Depolymerisation, and Upgrading. *Chem. Soc. Rev.* **2018**, *47*, 852−908.

(2) Zou, R.; Qian, M.; Wang, C.; Mateo, W.; Wang, Y.; Dai, L.; Lin, X.; Zhao, Y.; Huo, E.; Wang, L.; Zhang, X.; Kong, X.; Ruan, R.; Lei,

H. Biochar: From by-Products of Agro-Industrial Lignocellulosic Waste to Tailored Carbon-Based Catalysts for Biomass Thermochemical Conversions. *Chem. Eng. J.* **2022**, *441*, No. 135972.
(3) Gomes, G. R.; Scopel, E.; Rocha, N. L.; Breitkreitz, M. C.; Cormanich, R. A.; Rezende, C. A.; Pastre, J. C. Direct Ethyl Levulinate Production from Raw Lignocellulosic Biomass Mediated by a Novel Taurine-Based Imidazolium Ionic Liquid. *ACS Sustainable Chem. Eng.* **2022**, *10*, 15876−15888.
(4) Zhang, C.; Wang, F. Catalytic Lignin Depolymerization to Aromatic Chemicals. *Acc. Chem. Res.* **2020**, *53*, 470−484.
(5) Dong, L.; Lin, L. F.; Han, X.; Si, X. Q.; Liu, X. H.; Guo, Y.; Lu, F.; Rudic, S.; Parker, S. F.; Yang, S. H.; Wang, Y. Q. Breaking the Limit of Lignin Monomer Production via Cleavage of Interunit Carbon-Carbon Linkages. *Chem.* **2019**, *5*, 1521−1536.
(6) Yu, J.; Luo, B.; Wang, Y.; Wang, S.; Wu, K.; Liu, C.; Chu, S.; Zhang, H. An Efficient Way to Synthesize Biomass-Based Molybdenum Carbide Catalyst via Pyrolysis Carbonization and Its Application for Lignin Catalytic Pyrolysis. *Bioresour. Technol.* **2022**, *346*, No. 126640.
(7) Wang, H.; Pu, Y.; Ragauskas, A.; Yang, B. From Lignin to Valuable Products−Strategies, Challenges, and Prospects. *Bioresour. Technol.* **2019**, *271*, 449−461.
(8) Zakzeski, J.; Bruijnincx, P. C. A.; Jongerius, A. L.; Weckhuysen, B. M. The Catalytic Valorization of Lignin for the Production of Renewable Chemicals. *Chem. Rev.* **2010**, *110*, 3552−3599.
(9) Wu, W.; Luo, Z.; Liu, B.; Qiu, X.; Lin, J.; Sun, S.; Wang, X.; Lin, X.; Qin, Y. Zinc Vacancy Promotes Photo-Reforming Lignin Model to H_2 Evolution and Value-Added Chemicals Production. *Small Methods* **2023**, No. e2300462.
(10) Gao, P.; Li, C. Z.; Wang, H.; Wang, X. D.; Wang, A. Q. Perovskite Hollow Nanospheres for the Catalytic Wet Air Oxidation of Lignin. *Chin. J. Catal.* **2013**, *34*, 1811−1815.
(11) Chen, S.; Wang, W.; Li, X.; Yan, P.; Han, W.; Sheng, T.; Deng, T.; Zhu, W.; Wang, H. Regulating the Nanoscale Intimacy of Metal and Acidic Sites in Ru/γ-Al_2O_3 for the Selective Conversions of Lignin-Derived Phenols to Jet Fuels. *J. Energy Chem.* **2022**, *66*, 576−586.
(12) Fan, L. L.; Zhang, Y. N.; Liu, S. Y.; Zhou, N.; Chen, P.; Cheng, Y. L.; Addy, M.; Lu, Q.; Omar, M. M.; Liu, Y. H.; Wang, Y. P.; Dai, L. L.; Anderson, E.; Peng, P.; Lei, H. W.; Ruan, R. Bio-Oil from Fast Pyrolysis of Lignin: Effects of Process and Upgrading Parameters. *Bioresour. Technol.* **2017**, *241*, 1118−1126.
(13) Liu, E.; Segato, F.; Prade, R. A.; Wilkins, M. R. Exploring Lignin Depolymerization by A Bi-Enzyme System Containing Aryl Alcohol Oxidase and Lignin Peroxidase in Aqueous Biocompatible Ionic Liquids. *Bioresour. Technol.* **2021**, *338*, No. 125564.
(14) Yang, S.; Cai, G.; Lu, X.; Wang, C.; Feng, M.; Xu, J.; Zhou, Q.; Xin, J.; Ma, L. Selective Deoxygenation of Lignin-Derived Phenols and Dimeric Ethers with Protic Ionic Liquids. *Ind. Eng. Chem. Res.* **2020**, *59*, 4864−4871.
(15) Bjelić, A.; Grilc, M.; Likozar, B. Bifunctional Metallic-Acidic Mechanisms of Hydrodeoxygenation of Eugenol as Lignin Model Compound over Supported Cu, Ni, Pd, Pt, Rh and Ru Catalyst Materials. *Chem. Eng. J.* **2020**, *394*, No. 124914.
(16) Zeng, J.; Tong, Z.; Bao, H.; Chen, N.; Wang, F.; Wang, Y.; Xiao, D. Controllable Depolymerization of Lignin Using Carbocatalyst Graphene Oxide under Mild Conditions. *Fuel* **2020**, *267*, No. 117100.
(17) Lin, X.; Liu, J.; Qiu, X.; Liu, B.; Wang, X.; Chen, L.; Qin, Y. Ru−FeNi Alloy Heterojunctions on Lignin-derived Carbon as Bifunctional Electrocatalysts for Efficient Overall Water Splitting. *Angew. Chem., Int. Ed.* **2023**, *62* (33), No. e202306333.
(18) Lin, X.; Liu, J.; Wu, L.; Chen, L.; Qi, Y.; Qiu, Z.; Sun, S.; Dong, H.; Qiu, X.; Qin, Y. In situ Coupling of Lignin-Derived Carbon-Encapsulated CoFe-Co_xN Heterojunction for Oxygen Evolution Reaction. *AlChE J.* **2022**, *68*, No. e17785.
(19) Lin, X.; Fei, X.; Chen, D.; Qi, Y.; Xu, Q.; Liu, Y.; Zhang, Q.; Li, S.; Wang, T.; Qin, Y.; Qiu, X. Efficient Catalytic Upgrading of Ethanol to Higher Alcohols via Inhibiting C−C Cleavage and Promoting C−C Coupling over Biomass-Derived NiZn@NC Catalysts. *ACS Catal.* **2022**, *12*, 11573−11585.
(20) Kan, X.; Mi, J.; Zheng, Y.; Xiao, Y.; Liu, F.; Jiang, L. Gas-Template Directed in Situ Synthesis of Highly Nitrogen-Doped Carbon Nanotubes with Superior Sulfur Compatibility and Enhanced Functionalities. *Chem. Commun.* **2022**, *58*, 9290−9293.
(21) Kan, X.; Song, F.; Zhang, G.; Zheng, Y.; Zhu, Q.; Liu, F.; Jiang, L. Sustainable Design of Co-doped Ordered Mesoporous Carbons as Efficient and Long-lived Catalysts for H_2S Reutilization. *Chem. Eng. Sci.* **2023**, *269*, No. 118483.
(22) Kan, X.; Zhang, G.; Luo, Y.; Liu, F.; Zheng, Y.; Xiao, Y.; Cao, Y.; Au, C.-t.; Liang, S.; Jiang, L. Efficient Catalytic Removal of COS and H_2S over Graphitized 2D Micro-Meso-Macroporous Carbons Endowed with Ample Nitrogen Sites Synthesized via Mechanochemical Carbonization. *Green Energy Environ.* **2022**, *7*, 983−995.
(23) Li, C.; Li, H.; Wang, Y.; Tang, Z.; Shi, J.; Chen, M. Efficient Liquefaction of Kraft Lignin over N-doped Carbon Supported Size-Controlled MoC Nanoparticles in Supercritical Ethanol. *Fuel* **2023**, *333*, No. 126360.
(24) Ma, R.; Hao, W.; Ma, X.; Tian, Y.; Li, Y. Catalytic Ethanolysis of Kraft Lignin into High-Value Small-Molecular Chemicals over a Nanostructured α-Molybdenum Carbide Catalyst. *Angew. Chem., Int. Ed.* **2014**, *53*, 7310−7315.
(25) Wu, K.; Yang, C.; Zhu, Y.; Wang, J.; Wang, X.; Liu, C.; Liu, Y.; Lu, H.; Liang, B.; Li, Y. Synthesis-Controlled α- and β-Molybdenum Carbide for Base-Promoted Transfer Hydrogenation of Lignin to Aromatic Monomers in Ethanol. *Ind. Eng. Chem. Res.* **2019**, *58*, 20270−20281.
(26) Xiao, L. P.; Wang, S.; Li, H.; Li, Z.; Shi, Z. J.; Xiao, L.; Sun, R. C.; Fang, Y.; Song, G. Catalytic Hydrogenolysis of Lignins into Phenolic Compounds over Carbon Nanotube Supported Molybdenum Oxide. *ACS Catal.* **2017**, *7*, 7535−7542.
(27) Yan, B. C.; Lin, X. Y.; Chen, Z. H.; Cai, Q. J.; Zhang, S. P. Selective Production of Phenolic Monomers via High Efficient Lignin Depolymerization with A Carbon Based Nickel-Iron-Molybdenum Carbide Catalyst under Mild Conditions. *Bioresour. Technol.* **2021**, *321*, No. 124503.
(28) Wu, K.; Yang, C.; Liu, Y.; Liu, C.; Liu, Y.; Lu, H.; Liang, B. Hierarchical Meso- and Macroporous Carbon from Lignin for Kraft Lignin Decomposition to Aromatic Monomers. *Catal. Today* **2021**, *365*, 214−222.
(29) Kim, Y.; Jabed, M. A.; Price, D. M.; Kilin, D.; Kim, S. Toward Rational Design of Supported Vanadia Catalysts of Lignin Conversion to Phenol. *Chem. Eng. J.* **2022**, *446*, No. 136965.
(30) Yang, H.; Hita, I.; Wang, Z.; Winkelman, J. G. M.; Deuss, P. J.; Heeres, H. J. Solvent-Free Catalytic Hydrotreatment of Alcell Lignin Using Mono- and Bimetallic Ni(Mo) Catalysts Supported on Mesoporous Alumina. *ACS Sustainable Chem. Eng.* **2023**, *11*, 3170−3181.
(31) Cao, Y.; Gao, J.; Zhang, C.; Tsang, D. C. W.; Fan, J.; Clark, J. H.; Luo, G.; Zhu, X.; Zhang, S. Fast and Selective Production of Aromatics via Efficient Lignin Depolymerization: Critical Factors and Mechanism Studies. *ACS Sustainable Chem. Eng.* **2022**, *10*, 15273−15283.
(32) Graça, I.; Woodward, R. T.; Kennema, M.; Rinaldi, R. Formation and Fate of Carboxylic Acids in the Lignin-First Biorefining of Lignocellulose via H-Transfer Catalyzed by Raney Ni. *ACS Sustainable Chem. Eng.* **2018**, *6*, 13408−13419.
(33) Cronin, D. J.; Zhang, X.; Bartley, J.; Doherty, W. O. S. Lignin Depolymerization to Dicarboxylic Acids with Sodium Percarbonate. *ACS Sustainable Chem. Eng.* **2017**, *5*, 6253−6260.
(34) Cronin, D. J.; Dunn, K.; Zhang, X.; Doherty, W. O. S. Relating Dicarboxylic Acid Yield to Residual Lignin Structural Features. *ACS Sustainable. Chem. Eng.* **2017**, *5*, 11695−11705.
(35) Santana, C. S.; Aguiar, A. Effect of Lignin-Derived Methoxyphenols in Dye Decolorization by Fenton Systems. *Water Air Soil Pollut.* **2016**, *227* (2), No. 48, DOI: 10.1007/s11270-015-2703-0.

https://doi.org/10.1021/acs.iecr.3c01826
Ind. Eng. Chem. Res. 2023, 62, 13780−13789

(36) Zeng, J.; Yoo, C. G.; Wang, F.; Pan, X.; Vermerris, W.; Tong, Z. Biomimetic Fenton-Catalyzed Lignin Depolymerization to High-Value Aromatics and Dicarboxylic Acids. *ChemSusChem* **2015**, *8*, 861−871.
(37) Li, L.; Kong, J.; Zhang, H.; Liu, S.; Zeng, Q.; Zhang, Y.; Ma, H.; He, H.; Long, J.; Li, X. Selective Aerobic Oxidative Cleavage of Lignin C-C Bonds over Novel Hierarchical Ce-Cu/MFI Nanosheets. *Appl. Catal., B* **2020**, *279*, No. 119343.
(38) Cai, Z. P.; Long, J. X.; Li, Y. W.; Ye, L.; Yin, B. L.; France, L. J.; Dong, J. C.; Zheng, L. R.; He, H. Y.; Liu, S. J.; Tsang, S. C. E.; Li, X. H. Selective Production of Diethyl Maleate via Oxidative Cleavage of Lignin Aromatic Unit. *Chem.* **2019**, *5*, 2365−2377.
(39) Yadav, G. D.; Thathagar, M. B. Esterification of Maleic Acid with Ethanol over Cation-Exchange Resin Catalysts. *React. Funct. Polym.* **2002**, *52*, 99−110.
(40) Cattelan, L.; Yuen, A. K. L.; Lui, M. Y.; Masters, A. F.; Selva, M.; Perosa, A.; Maschmeyer, T. Renewable Aromatics from Kraft Lignin with Molybdenum-Based Catalysts. *ChemCatChem* **2017**, *9*, 2717−2726.
(41) Wu, K.; Sang, Y.; Kasipandi, S.; Ma, Y.; Jiao, H.; Liu, Q.; Chen, H.; Li, Y. Catalytic Roles of Mo-Based Sites on MoS_2 for Ethanolysis of Enzymatic Hydrolysis Lignin into Aromatic Monomers. *Catal. Today* **2023**, *408*, 211−222.
(42) Bau, J. A.; Emwas, A.-H.; Nikolaienko, P.; Aljarb, A. A.; Tung, V.; Rueping, M. Mo^{3+} Hydride as the Common Origin of H_2 Evolution and Selective NADH Regeneration in Molybdenum Sulfide Electrocatalysts. *Nat. Catal.* **2022**, *5*, 397−404.
(43) Wang, W.; Huang, J.; Fu, Y.; Jiang, W.; Chen, Y.; Ma, Y.; Han, S. A 3D Porous Fe-MoS_2/CMF Catalyst for High-Efficient Catalytic Reforming of Lignin Vapor by Microwave Irradiation. *Appl. Catal., B* **2023**, *333*, No. 122787.
(44) Grilc, M.; Veryasov, G.; Likozar, B.; Jesih, A.; Levec, J. Hydrodeoxygenation of Solvolysed Lignocellulosic Biomass by Unsupported MoS_2, MoO_2, Mo_2C and WS_2 Catalysts. *Appl. Catal., B* **2015**, *163*, 467−477.
(45) Chen, W. T.; Han, S.; Gao, Z. T.; Sun, M. S.; Li, Z. M.; Tao, D. J. B/N co-Doped Carbon Supported Molybdenum Carbide Catalysts with Oxygen Vacancies for Facile Synthesis of Flavones through Oxidative Dehydrogenation. *J. Colloid Interface Sci.* **2022**, *623*, 735−743.
(46) Wang, D.; Cui, M.; Zhao, W.; Li, Y.; Ma, S.; Jiang, Z.; Liu, X.; Liang, C.; Li, R.; Ma, L.; Song, Y.; Wei, X. Y. Production of Diethyl Maleate via Oxidative Depolymerization of Organosolv Lignin from Wheat Stalk over the Cooperative Acidic Ionic Liquid Pair. *J. Agric. Food Chem.* **2023**, *71*, 3800−3812.
(47) Li, Z. M.; Long, J. X.; Zeng, Q.; Wu, Y. H.; Cao, M. L.; Liu, S. J.; Li, X. H. Production of Methyl p-Hydroxycinnamate by Selective Tailoring of Herbaceous Lignin Using Metal-Based Deep Eutectic Solvents (DES) as Catalyst. *Ind. Eng. Chem. Res.* **2020**, *59*, 17328−17337.
(48) Li, Z. M.; Cai, Z. P.; Zeng, Q.; Zhang, T.; France, L. J.; Song, C. H.; Zhang, Y. Q.; He, H. Y.; Jiang, L. L.; Long, J. X.; Li, X. H. Selective Catalytic Tailoring of the H Unit in Herbaceous Lignin for Methyl p-Hydroxycinnamate Production over Metal-Based Ionic Liquids. *Green Chem.* **2018**, *20*, 3743−3752.
(49) Lancefield, C. S.; Ojo, O. S.; Tran, F.; Westwood, N. J. Isolation of Functionalized Phenolic Monomers through Selective Oxidation and C-O Bond Cleavage of the Beta-O-4 Linkages in Lignin. *Angew. Chem., Int. Ed.* **2015**, *54*, 258−262.
(50) Lan, W.; Amiri, M. T.; Hunston, C. M.; Luterbacher, J. S. Protection Group Effects during α,γ-Diol Lignin Stabilization Promote High-Selectivity Monomer Production. *Angew. Chem. Int. Ed.*. **2018**, *57*, 1356−1360.
(51) Li, Y. D.; Li, S.; Kim, H.; Motagamwala, A. H.; Mobley, J. K.; Yue, F.; Tobimatsu, Y.; Havkin-Frenkel, D.; Chen, F.; Dixon, R. A.; Luterbacher, J. S.; Dumesic, J. A.; Ralph, J. An "Ideal Lignin" Facilitates full Biomass Utilization. *Sci. Adv.* **2018**, *4*, No. eaau2968.
(52) Wu, X. J.; Fan, X. T.; Xie, S. J.; Lin, J. C.; Cheng, J.; Zhang, Q. H.; Chen, L. Y.; Wang, Y. Solar Energy-Driven Lignin-First Approach to Full Utilization of Lignocellulosic Biomass under Mild Conditions. *Nat. Catal.* **2018**, *1*, 772−780.

https://doi.org/10.1021/acs.iecr.3c01826
Ind. Eng. Chem. Res. 2023, 62, 13780−13789